Void growth and coalescence in a three-dimensional non-periodic void cluster

Victor-Manuel Trejo-Navas, Marc Bernacki, Pierre-Olivier Bouchard

Void growth and coalescence in a three-dimensional non-periodic void cluster

Trejo Navas, Victor Manuel Bernacki, Marc
Bouchard, Pierre-Olivier

January 16, 2018

Abstract

Void growth and coalescence are studied in this work through Finite Element simulations. A methodology for the study of three-dimensional non-periodic configurations is proposed. In order to avoid the hypothesis of microstructural periodicity, a three-dimensional cluster with three initially spherical voids, is modeled. Multiple spatial configurations are simulated in a parametric study. The pre-coalescence behavior is detailed through the evolution of the volume of each void, the minimum intervoid distance, and the equivalent plastic strain in the middle of the shortest path between voids, and the resulting coalescence mechanism is described. Locally accelerated and non-homogeneous void growth is observed close to the localization band. Although only coalescence by internal necking is present, apparent void-sheet formation is observed if only a two-dimensional slice is considered. These observations, and a comparison with the Rice-Tracey growth model, highlight the importance of fully considering the three-dimensional complexity of the ductile damage micromechanisms.

1 Introduction

A better understanding of ductile damage can enhance the accuracy of fracture prediction during in-use life, optimize designs of mechanical pieces, and improve forming processes. Further improving the understanding of the micromechanisms of ductile damage -void nucleation, growth, and coalescence- is essential for the development of more predictive and universal macroscopic models. This paper focuses on void growth and on void coalescence mechanisms.

Void coalescence is usually categorized into three different mechanisms [1, 2]. The first and most common mechanism is coalescence by internal necking of the intervoid ligament. In the second mechanism, two voids seemingly wide apart, are suddenly united by a narrow void sheet. This is referred to as void-sheet mechanism. The third and less common mechanism is known as necklace coalescence or coalescence in columns, in which voids link up along their length.

Void-sheet coalescence was observed by Cox and Low [3] in an AISI 4350 alloy (see Figure 1). The authors identified these void sheets as planar features formed by small voids, and oriented at 45° with respect to the tensile axis. The orientation of this feature coincides with the direction of maximum shear. This void-sheet mechanism can have a negative impact on the ductility of the material [3, 4].

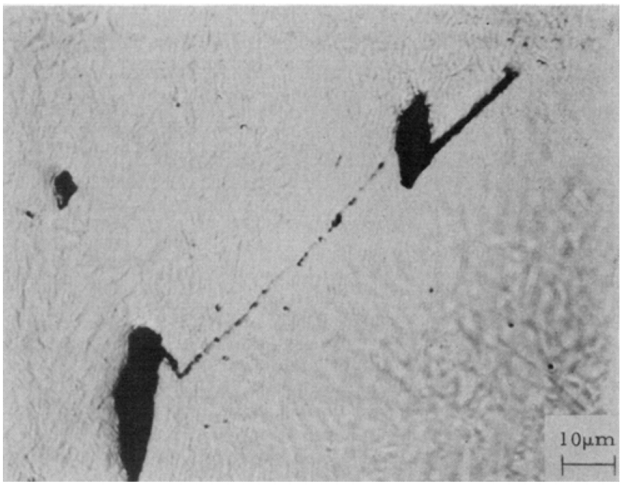

Figure 1: Instance of void-sheet mechanism observed by Cox and Low [3] in an AISI 4350 alloy.

Recent efforts have employed three-dimensional imaging techniques, such as X-ray tomography or Synchrotron radiation computing tomography (SRCT), to study and improve the understanding of ductile damage mechanisms [5, 6, 7, 8].

Babout et al [9] studied damage in model metallic materials via X-ray tomography by carrying out in situ tensile tests in two different aluminum matrices reinforced with spherical hard ceramic particles. The authors observed coalescence (Figure 2) in the highest strained regions between voids at approximately 45 deg from the tensile direction.

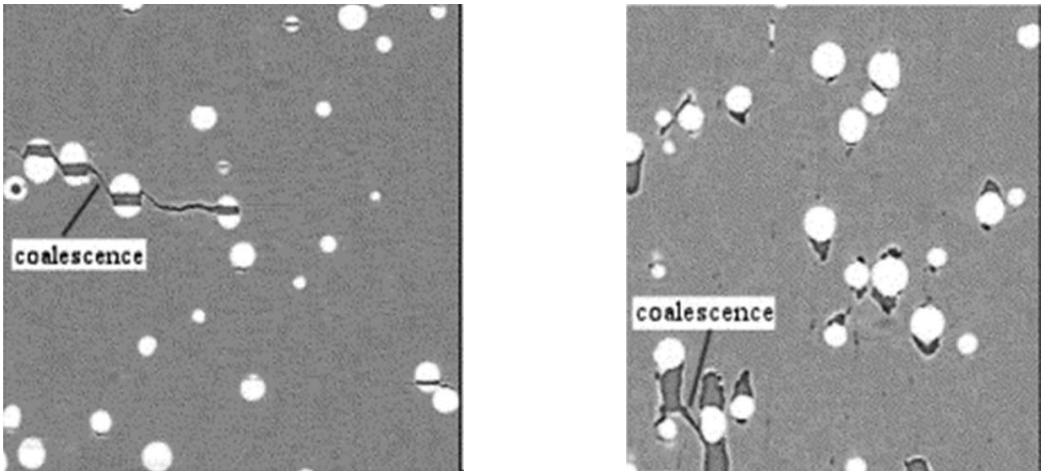

(a) Hard matrix (b) Soft matrix

Figure 2: Coalescence instances observed by Babout et al. [9]. Figures adapted from [9].

In the analysis of SRCT images of a commercial nodular graphite cast iron (EN-GJS-400) [10, 11], various instances of apparent void-sheet coalescence have been observed. Two examples of these instances are presented in Figure 3. The tensile direction corresponds to the vertical direction. The specimen presents two holes created via Electrical Discharge Machining (EDM) to favor shear conditions between the holes. Two coalescence instances are indicated in red in Figure 3b. Even though the two-dimensional images suggest the occurrence of the void-sheet mechanism, the three-dimensional images hint at a possible intervention of voids located close to the observed coalescence; the objective of this work is to numerically investigate the possible intervention of neighboring voids. More details on damage and failure mechanisms of this material can be found in the works of Buljac et al [12].

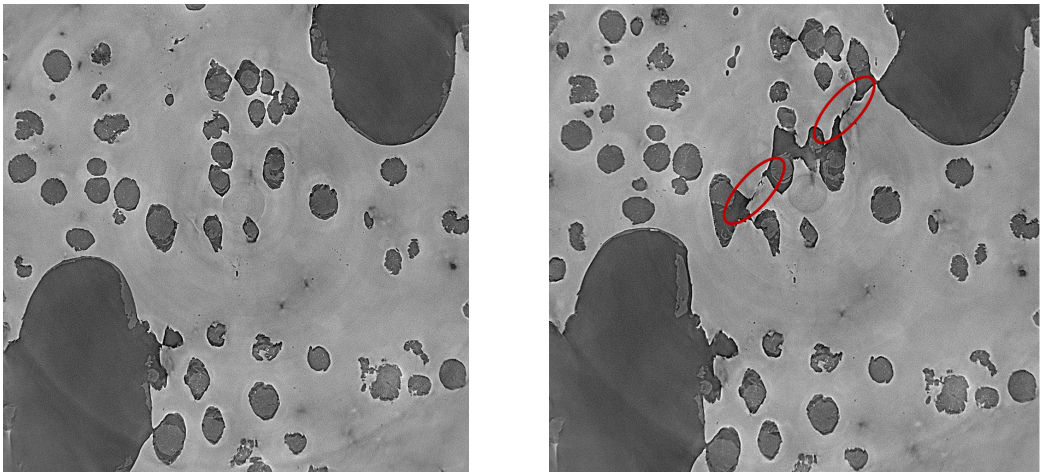

(a) Before coalescence (b) After coalescence

Figure 3: Apparent void-sheet instance observed in a two-dimensional slice of a laminography scan of nodular cast iron [10, 11].

To investigate three-dimensional effects on the apparent void-sheet mechanisms observed in different materials, Finite element (FE) simulations are carried out. A three-dimensional non-periodic cluster of three voids is investigated in a parametric study. Since a classical unit-cell approach is not suitable for this task, a methodology for the study of three-dimensional non-periodic clusters of voids and/or particles is proposed. In section 2, the numerical framework, the proposed methodology and the parametric study are described. Results are presented and discussed in Section 3, and conclusions are drawn in Section 4.

2 Methodology

2.1 Numerical framework

Since the used numerical framework has been sufficiently documented in previous publications [13, 14], only a brief description is given here.

The multiphase FE simulations are carried out with a Lagrangian formulation and a monolithic approach, i.e., on a single mesh. The void-matrix interface is described by the zero isovalue of a distance function. The distance function is convected with the Lagrangian mesh motion and, when necessary, reinitialized with an efficient and parallel algorithm [15]. Body-fitted meshing and remeshing operations are performed when necessary with an excellent conservation of the void phase [14]. The way in which coalescence is handled in the FE mesh, has been treated in detail in previous work [14]. The matrix is considered elasto-perfectly plastic (Young's modulus $E = 210000$MPa, Poisson's ratio $\nu = 0.3$ and yield stress $\sigma_y = 290$MPa) and the void phase is modeled as a compressible Newtonian fluid (viscosity $\eta = 2.1$MPa s^{-1}); this approach has been previously validated [16]. A mixed velocity/pressure formulation with a P1+/P1 element is used [17]. Sensitivity analyses with respect to the temporal and spatial discretizations were carried out in order to find optimal parameters in terms of precision and numerical cost. As in the work of Roux et al. [16], an additional sensitivity analysis was carried out to verify that the mechanical properties of the void phase, and the resulting internal pressure in the voids, bears no influence on the considered observables.

2.2 Methodology for the study of void and/or inclusion clusters

2.2.1 Motivation

The unit-cell approach [18, 19] has been very important in the development of the local approach to fracture. A great number of studies have been and continue to be carried out with this approach. Typically, in the unit-cell approach, a single inclusion or void is embedded in a unit-cell surrounded by periodic boundary conditions. This greatly simplifies the study of the micromechanisms of ductile damage and allows the effect of many microstructural variables to be assessed. Doing so, however, imposes an important simplifying hypothesis: that the studied microstructure can be represented by a periodic arrange of microstructural features.

The hypothesis of a periodic microstructure is not always an appropriate approximation. This constitutes a compelling reason to enrich the available tools and methodologies for the study of ductile damage. Within the unit-cell framework, different works have extended the original framework by considering unit-cells with multiple voids/particles. Thomson et al. [20] studied the effect of the orientation of a particle cluster with respect to the main loading direction, on void nucleation and growth. The study was later extended to assess void coalescence [21]. McVeigh et al. [22] studied the onset of the void-sheet mechanism with a unit-cell submitted to shear loading. In plane strain conditions, Tvergaard compared clusters with different numbers of voids, but equal total void volume, and concluded that void clusters grow more rapidly [23]. The role of secondary voids and their spatial distribution on void growth and coalescence was assessed by Khan and Bhasin [24].

A second group of studies has investigated non-uniform distributions of voids without recurring to the unit-cell approach. Ohno and Hutchinson [25] studied the effect of void clustering on plastic flow localization by modeling

a band of non-uniformly distributed voids between two bands of homogeneous material. Horstemeyer et al. [26] quantified coalescence effects based on temperature for different arrangements of voids. Bandstra and Koss [27] investigated void-sheet coalescence with a computational model of two voids for stress state and proposed a critical local strain value for the onset of void-sheet coalescence based on the nucleation strain for secondary particles. Bandstra et al. [28] examined the deformation localization behavior with void arrays based on experimentally observed microstructures. Tvergaard and Needleman [29] assessed the effect of two populations of second-phase particles on crack growth. Bandstra and Koss [30] assessed the sensitivity of void growth and coalescence to intervoid spacing. Shakoor et al. [13] compared uniform and random arrangements of voids to investigate the resulting difference in ductility.

A third group of works has focused on modeling realistic microstructures based on experimental images. Sun et al. [31] modeled an actual microstructure based on scanning electron microscrope (SEM) image, under plane stress conditions. Vanderesse et al. [32] meshed a volumetric image obtained by X-ray microtomography and carried out FE simulations. Padilla et al. [33] carried out FE simulations of a microstructure obtained via X-ray microtomography in order to assess the evolution of damage in a single lap shear joint. Buljac et al. [10] used synchrotron 3D imaging to immerse microstructures and carry out FE analyses with realistic boundary conditions [11] obtained via digital volume correlation (DVC) and in-situ laminography tests.

The use of three-dimensional imaging in conjunction with FE modeling brings about opportunities to study ductile damage in more realistic situations. This increase in realism implies an increase in complexity and microstructural parameters are observed rather than controlled. For example, in a typical unit-cell, the intervoid distance is constant and imposed with the cell geometry; in a FE analysis of an immersed microstructure, an intervoid distance distribution is obtained when the image is immersed. To verify an hypothesis or investigate a specific effect without necessarily recurring to pe-

riodic arrangements and idealized shapes, it might be desirable 1. to control a given microstructural variable or 2. to study a certain isolated configuration or clusters of voids and/or particles. This is the main motivation for the methodology proposed in this work.

2.2.2 Description

A methodology for the study of void and/or inclusion clusters, is proposed here as a complement to FE analysis of realistic microstructures. It has the following defining characteristics:

- Dedicated to the study of void and/or inclusion non-periodic clusters.
- Possibility of using microstructural features of non-idealized shapes.
- Reference to a far-field stress.
- The calculations can be controlled with a given stress state in terms of stress triaxiality ratio and Lode parameter.
- Possibility of imposing arbitrary non-proportional loadings.
- Possibility of obtaining detailed information of the studied configuration (See Section 3 for an example).

A domain with an embedded microstructural configuration is modeled. The size of the domain is considerably larger than the embedded configuration to assure negligible interaction with the boundaries. The microstructural configuration analyzed in this study is depicted in Figure 4a.

The cubic domain is depicted in Figure 4b and the boundary conditions are schematized. Three symmetry planes are used (red arrows in Figure 4b). The vertical velocity is imposed on the top plane (green arrow in Figure 4b), and is calculated to impose a given vertical logarithmic strain. The

horizontal velocities corresponding to the perpendicular directions of the two remaining faces (blue arrows in Figure 4b) are imposed. In order to obtain a desired stress state in the domain, these horizontal velocities are iteratively calculated during the simulations via an optimization algorithm. A simplex algorithm [34] implemented in the open-source nonlinear-optimization library NLopt [35] and coupled with CimLib [36], was used. The stress state is imposed in terms of stress triaxiality ratio T and normalized Lode angle $\bar{\theta}$. For all the simulations presented here, constant values of $T = 1$ and $\bar{\theta} = 0.34$ were used; a high triaxiality value was chosen to promote void growth, and value of the normalized Lode angle is similar to those found locally in the vicinity of void-sheet like instances in micromechanical FE simulations with immersed microstructures and realistic boundary conditions such as those documented in the work of Shakoor et al. [11].

The described methodology differentiates itself from unit-cell studies such as, for example, the works of Tvergaard [23] or Khan and Bhasin [24], by its focus on a isolated non-periodic void cluster. Although the applied boundary conditions result in periodicity, the relative size of the void cluster with respect to the domain ensures that the interaction with the boundaries is inconsequential.

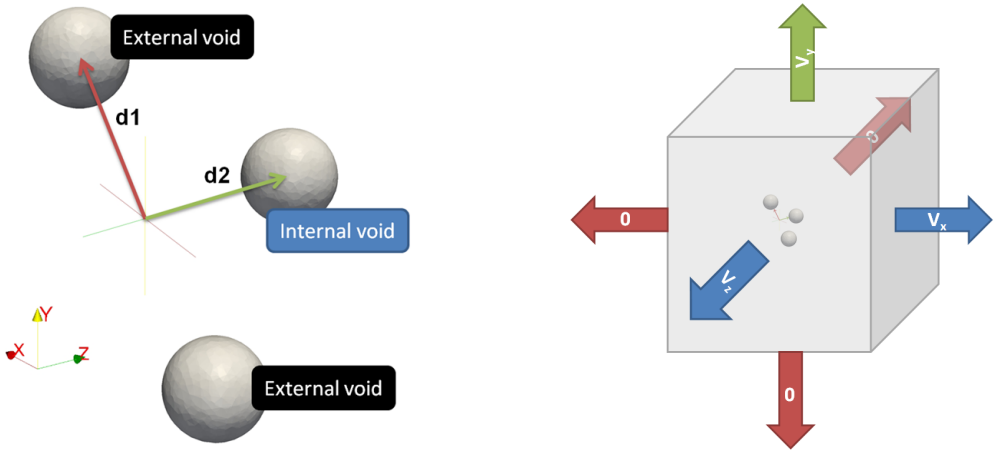

(a) (b)

Figure 4: (a) Scheme of initial configurations of the three voids and (b) scheme of computational domain.

2.3 Parametric study

This parametric study has two objectives. The first one is to provide a general description of the behavior of a three voids cluster during the stages of growth and coalescence. The second objective is to assess if such a configuration can be related to the observed instances of void-sheet coalescence (See section 1). In this study, the term coalescence refers to actual void impingement and not to the plastic localization stage that precedes it. A pair of voids is herein said to undergo coalescence when the intervoid distance reaches zero.

2.3.1 Studied configuration

The three voids cluster is depicted in Figure 4a. It is constituted by three voids with a radius $R = 50\mu m$: two of them will be referred to as external voids and the third one will be referred to as the internal void. The line that

Table 1: Explored parametric space.

d1\d2 [-]	1	1.75	2.5	3.25	4
1	☒	☒	☒	☒	☒
1.75	☒	☒	☒		☒
2.5	☒	☒		☒	☒
3.25		☒	☒		☒

connects the centers of the two external voids forms 45° with the main loading direction (the vertical direction). The vertical position (y-direction) of the center of the internal void is located exactly at mid-height of the domain and hence between the two external voids. The internal void is shifted in the thickness direction (z-direction) by a given distance.

2.3.2 Parameters

To construct different initial configurations, the relative positions of the voids in the three voids cluster were described with two parameters, which are depicted in Figure 4a along with a scheme of a given initial configuration. The two adimensional parameters are: d_1 the distance between the center of the domain and the center of the external voids divided by R, and d_2, the distance between the center of the domain and the center of the internal void divided by R.

The explored parametric space is summarized in Table 1; the accomplished simulations are indicated by a cross. A total of 16 simulations were carried out. The range between 1 and 3.25 was used for d_1, and the range between 1 and 4 was used for d_2.

3 Results

Results for a single simulation with $d_1 = 1$ and $d_2 = 1$ are first discussed in Section 3.1. Subsequently, the results of the parametric study are presented in Sections 3.2, 3.3 and 3.4.

3.1 Results for the case with $d_1 = 1$ and $d_2 = 1$

The results for the case with $d_1 = 1$ and $d_2 = 1$, indicated in red in Table 1, are now discussed. A plastic localization band, shown in Figure 5 at 0.7% of imposed macroscopic equivalent strain, is formed between the two external voids. The internal void presents a heterogeneous growth acceleration. The preferred growth direction points towards the position of the acceleration band between the external voids. These accelerated void growth eventually leads to coalescence by internal necking between the internal void and the external voids.

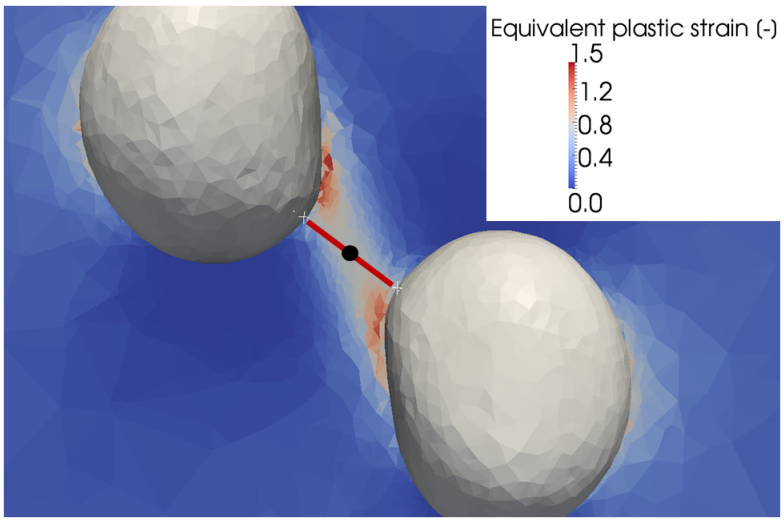

Figure 5: Strain localization band in a plane containing the external voids at 0.7% of imposed macroscopic equivalent strain. The minimum intervoid distance is indicated by a red line and its middle point by a black dot.

Figure 6a shows a three-dimensional view of the voids after coalescence at 0.13% of macroscopic equivalent strain. The shape of the internal void significantly deviates from a spheroidal shape; the void develops a high curvature zone that extends towards the strain localization band between the external voids. This deviation puts in evidence the heterogeneous acceleration of void growth due to the interaction with the external voids.

Figure 6b presents a two-dimensional cut of the same simulation also after coalescence at 0.13% of macroscopic equivalent strain. In this depiction of the void arrangement, the bulk of the internal void cannot be seen. Instead, a narrow void band between the external voids is visible. This narrow region is the part of the internal void that coincides with the shown cross-section. If only this image of the void arrangement is available and the presence of a third void is ignored, it might be interpreted as an instance of void-sheet coalescence. This supports the hypothesis that three-dimensional interactions between voids can produce coalescence of multiple voids that highly resemble the void-sheet mechanism if observed from a two-dimensional perspective.

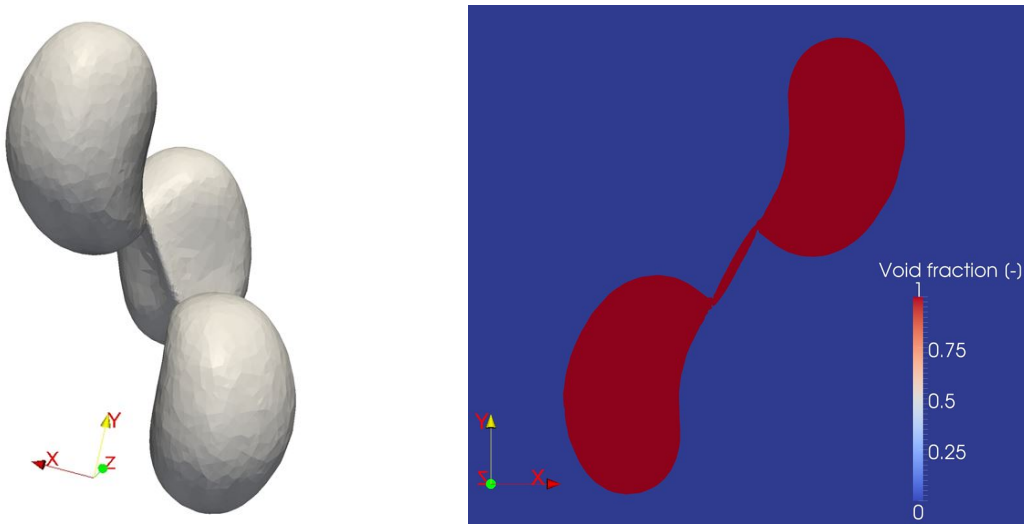

(a) Three-dimensional view

(b) Two-dimensional view

Figure 6: Configuration of voids after coalescence at 0.13% of macroscopic equivalent strain for $d_1 = 1$ and $d_2 = 1$.

This coalescence mechanism between 3 voids will be described by considering three observables: the normalized void volume of each void (Figure 7), the minimum intervoid distance for each pair of voids (Figure 8) , and the equivalent plastic strain at the middle point of the shortest path between each pair of voids (Figure 9). The minimum intervoid distance and the middle point of the shortest path are schematized in Figure 5 for a pair of voids with a red line and a black dot, respectively.

In Figure 7, the normalized void volume is presented for each void as a function of the imposed macroscopic equivalent strain ε_{yy}; the end of the curves corresponds to the value of ε_{yy} at the moment of coalescence. The behavior of the two external voids is identical since there is no asymmetry to differentiate them. The internal void, however, presents an accelerated void growth that, at coalescence, represents an additional 10% volume increase with respect to the external voids. Since all the voids are subject to the same macroscopic stress state, it is the local differences of stress state, i.e., the interaction with the external voids, that induce this accelerated void growth and promote the formation of the observed high curvature zone (Figure 6a). This high curvature region will, in turn, modify the stress state ahead of the resulting notch-like feature and further accelerate void growth.

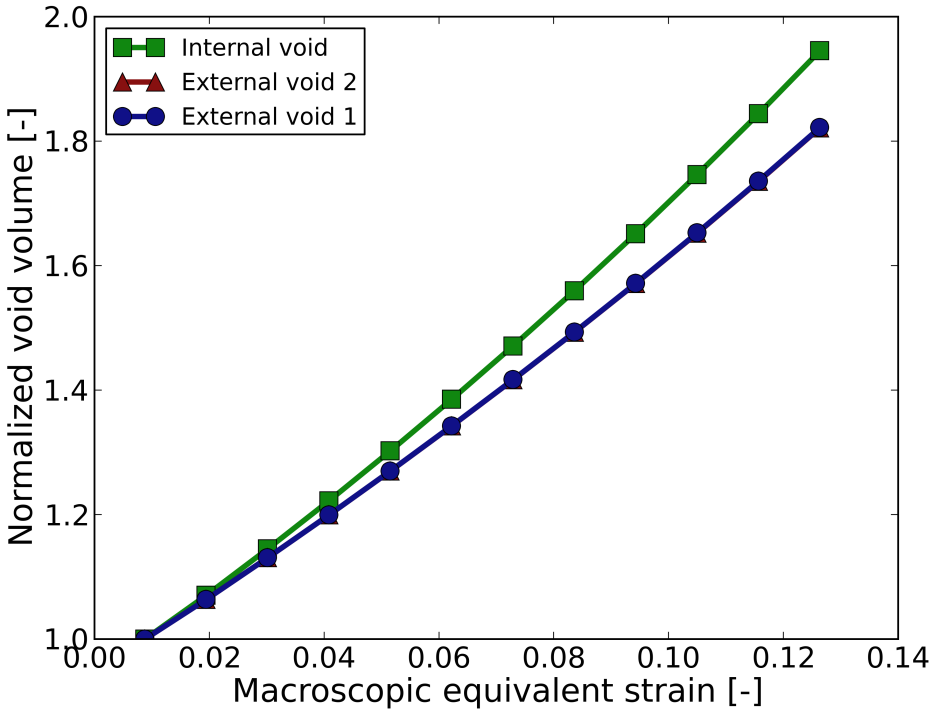

Figure 7: Normalized void volume for $d_1 = 1$ and $d_2 = 1$.

Since the behavior of the two external voids is identical, only two pairs of voids are considered in the following: the external-external pair and one of the two internal-external pairs. Figure 8 presents the evolution up to coalescence of the minimum intervoid distance for these two pairs of voids. As the domain is deformed, both curves decrease monotonically and almost linearly with nearly identical rates of decrease. The internal-external pairs experience coalescence when their minimum intervoid distance approaches zero.

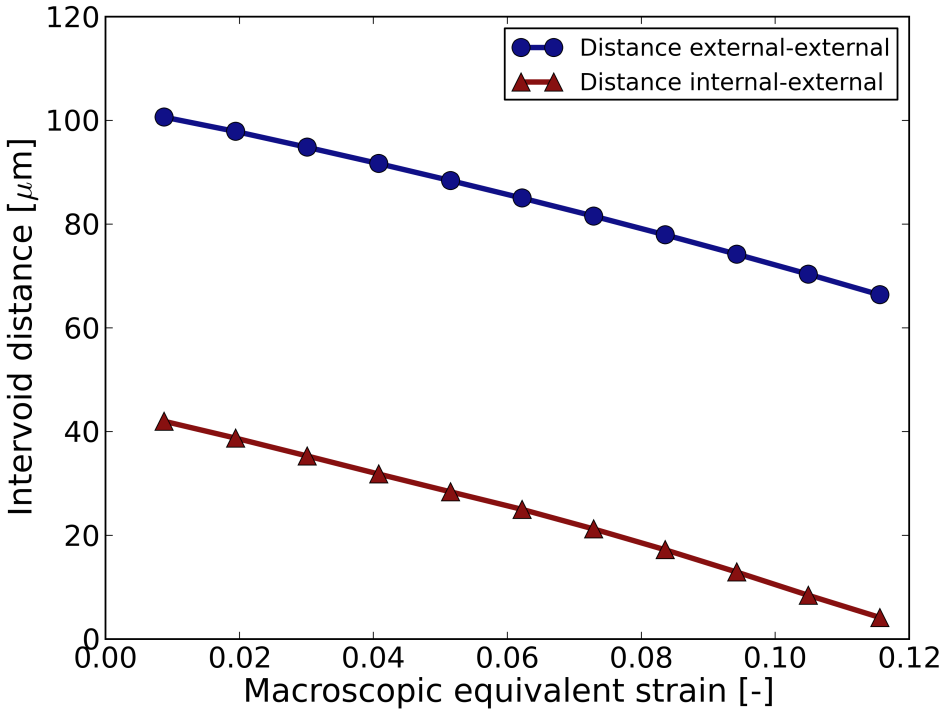

Figure 8: Minimum intervoid distance for $d_1 = 1$ and $d_2 = 1$.

Figure 9 exhibits the evolution of the plastic strain at the middle point of the shortest path between voids. At the middle point of the external-external pair, the equivalent strain evolves linearly with a slope of approximately 7.8, i.e., even if no exponential trend is observed, this local strain increases a lot more rapidly than the strain imposed on the domain. The equivalent strain at the middle point of the internal-external pair increases exponentially. This is consistent with the observed final configuration since it is the internal-external pair that undergoes coalescence by internal necking. Coalescence occurs at a macroscopic equivalent strain of 0.11.

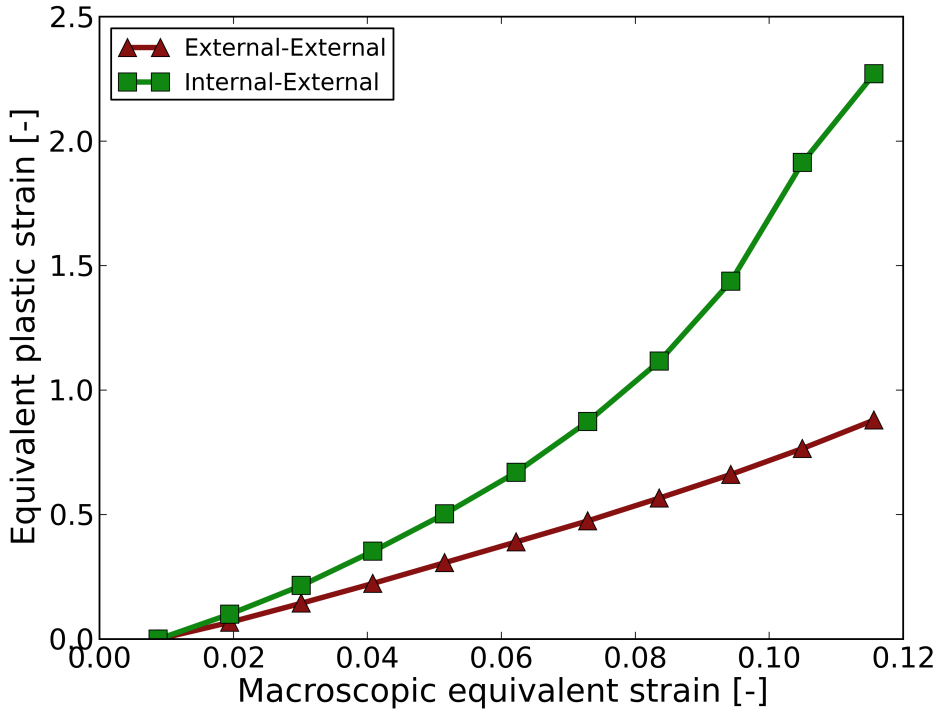

Figure 9: Equivalent plastic strain at middle point of shortest path between voids for $d_1 = 1$ and $d_2 = 1$.

The analysis of the case with $d_1 = 1$ and $d_2 = 1$ provided evidence of the heterogeneous void growth that results from the interaction between the three voids in the cluster. The coalescence of the cluster was described through three observables: the normalized void growth, the minimum inter-void distance and the equivalent strain at the middle point of the shortest path between each pair of voids. Sections 3.2 and 3.3 investigate further the described coalescence mechanism by exploring how these three observables evolve when the relative positions of the voids in the cluster change.

3.2 Effect of d_2

The effect of d_2 is examined in this subsection, i.e., the position of the external voids is fixed ($d_1 = 1$), and the effect of changing the position of the internal void is examined. This corresponds to exploring the design space in the sense indicated in blue in Table 1. The evolution of void volume, intervoid distance and local plastic strain as functions of the macroscopic equivalent strain, change with increasing d_2. These evolutions are described in Figures 10, 11 and 12, respectively. Figure 13 presents three-dimensional views of the voids just after coalescence.

As described in section 3.1, the case with $d_2 = 1$ (Figure 10a) presents a linear evolution in terms of void volume. When d_2 increases, the void volume evolution changes and presents an exponential behavior. The $d_2 = 1$ case (Figure 10a) presents a normalized void growth of about 1.95 for the internal void at coalescence, and it increases up to 7.8 for the case with $d_2 = 4$ (Figure 10d).

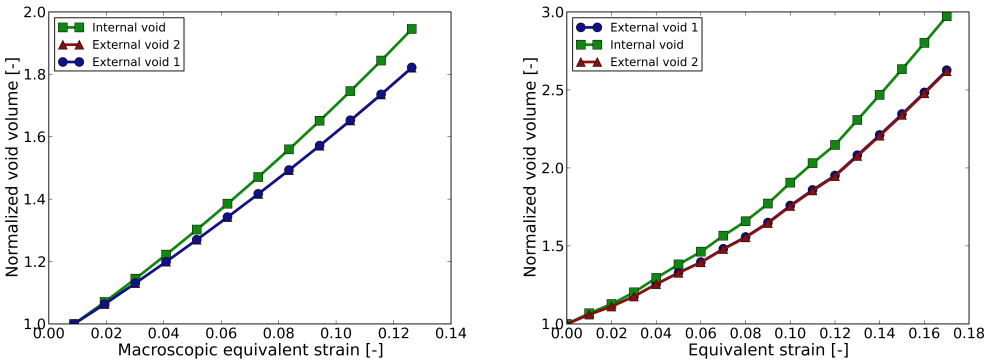

(a) $d_2 = 1$ (b) $d_2 = 1.75$

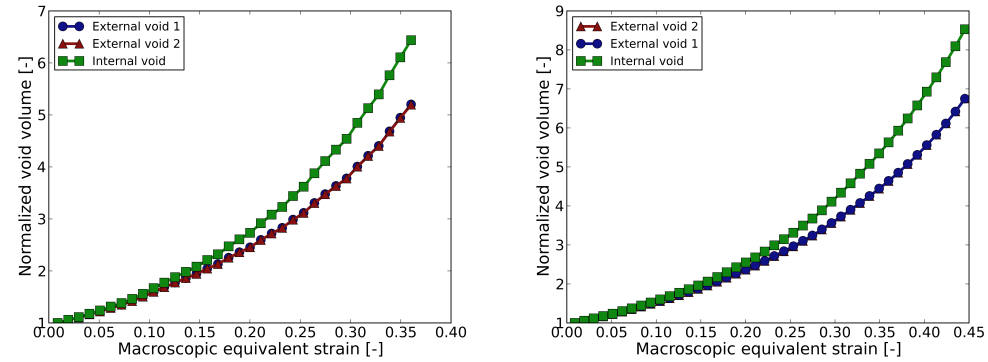

(c) $d_2 = 3.25$ (d) $d_2 = 4$

Figure 10: Effect of d_2 on the normalized void volume for a fixed value of $d1 = 1$.

Even when d_2 is 4 times d_1, the internal void presents more void growth than the external voids. Since all voids are subject to the same macroscopic stress state, this shows that amount of void growth undergone by a given void can be a complex function of its position in a given void cluster.

The evolution of the relationship intervoid distance-macroscopic equivalent strain is depicted in Figure 11. In the same manner as for the normalized void volume, the linear behavior of the intervoid distance observed for $d_2 = 1$ disappears when d_2 increases.

For the cases with $d_2 = 1$ (Figure 11a) and $d_2 = 1.75$ (Figure 11b), the internal-external pair of voids are closer in the initial configuration and coalesces first. Also for the case $d_2 = 3.25$ (Figure 11c), coalescence of the internal-external pair is observed first even if the initial intervoid distance of this pair represents approximately 140% of the intervoid distance of the external-external pair. For the case $d_2 = 4$ (Figure 11d), the initial intervoid distance of the internal-external pair is 160% that of the external-external pair, and a simultaneous coalescence between the 3 voids is observed (Figure 13d).

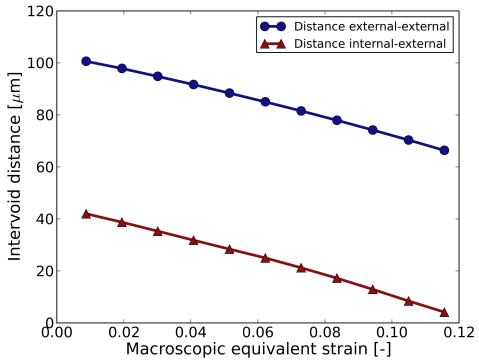

(a) $d_2 = 1$

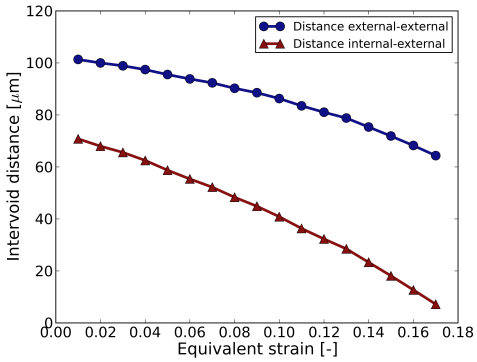

(b) $d_2 = 1.75$

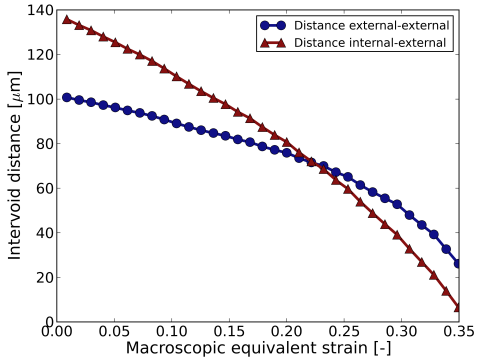

(c) $d_2 = 3.25$

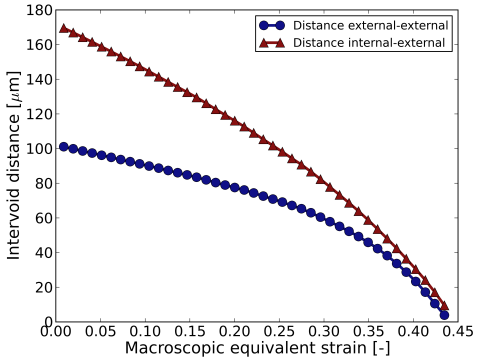

(d) $d_2 = 4$

Figure 11: Effect of d_2 on the minimum intervoid distance for a fixed value of $d1 = 1$.

Figure 12 presents the evolution the equivalent plastic strain at the middle point of the shortest path between each pair of voids, for four different values of d_2. The last value of the macroscopic equivalent strain of each pair of curves represents the value for which coalescence was observed; it increases monotonically with d_2, and goes from 0.11 (Figure 12a) to 0.39 (Figure 12d). Irrespectively of the value of the macroscopic equivalent strain, the local strain just before coalescence is in the range of 2.5-3.0

The plastic strain in the middle of the internal-external pair behaves exponentially for all four cases. For the the external-external pair, it goes from a linear behavior to an exponential behavior as d_2 increases, and it is practically superimposed with that of the internal-external pair when d_2 reaches a value of 4.

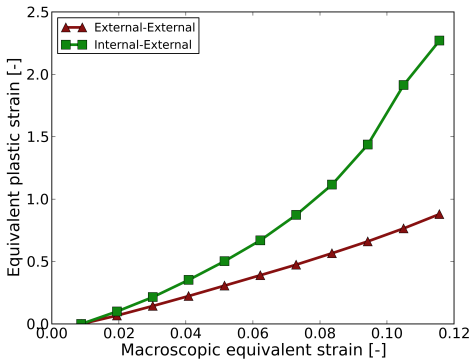

(a) $d_2 = 1$

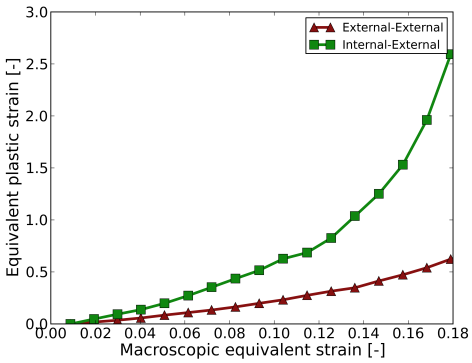

(b) $d_2 = 1.75$

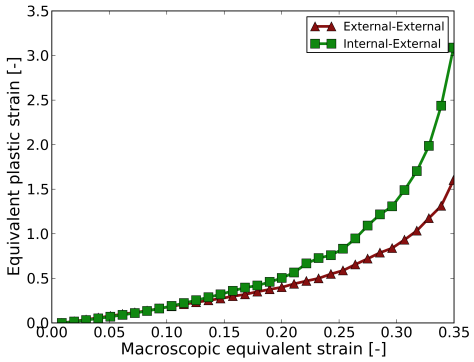

(c) $d_2 = 3.25$

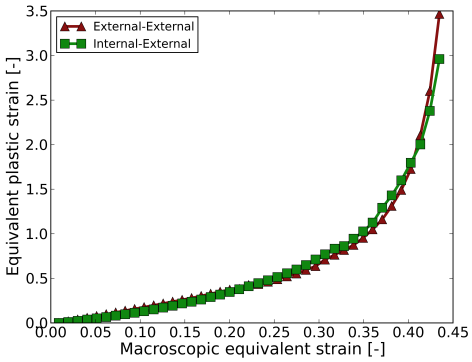

(d) $d_2 = 4$

Figure 12: Effect of d_2 on the equivalent plastic strain at middle point of shortest path between voids for a fixed value of $d1 = 1$.

Figure 13 presents three-dimensional views of the configuration of the voids just after coalescence for the four cases described in this section. The perspective in each image was adjusted to try to capture well the resulting arrangement. The notch-like feature resulting from the formation of the high curvature region is present in all four cases even if the void shapes vary considerably between the different configurations. For d_2 inferior to 4, the coalescence by internal necking is observed between the internal-external pairs. For $d_2 = 4$ simultaneous coalescence between the three voids is obtained.

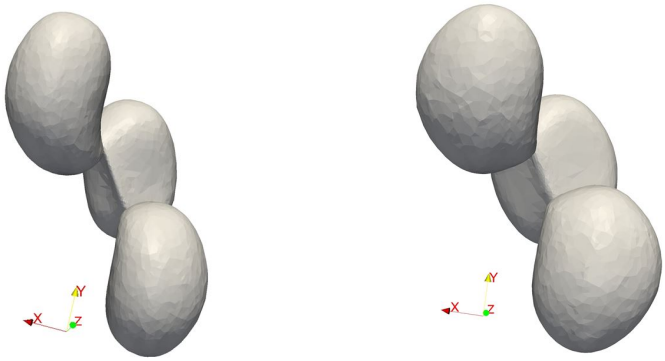

(a) $d_2 = 1$ (b) $d_2 = 1.75$

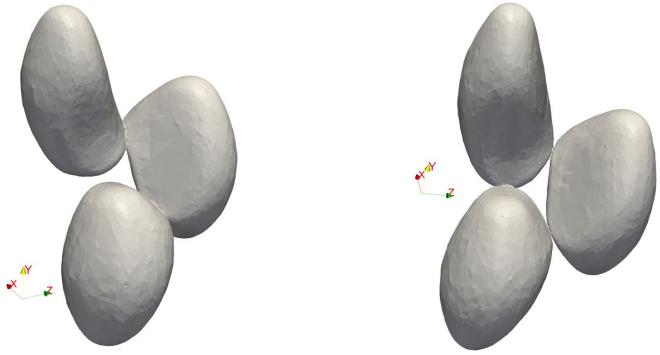

(c) $d_2 = 3.25$ (d) $d_2 = 4$

Figure 13: Final configuration of voids after coalescence for $d_1 = 1$ and different values of d_2.

3.2.1 Effect of the internal void on void growth

In this section, the effect of the presence of the internal void on void growth is studied. Figure 14 presents the normalized void volume of the external voids for different values of d_2 and a fixed value of $d_1 = 1$. As the internal void moves away from the void cluster, the external void grows more slowly and the domain deforms further before coalescence. In the limit case, the internal void is so far away from the cluster that there is no more influence if this void on the growth of the external voids. This case was modeled by simulating only the two external voids in absence of the internal void and is

also represented in Figure 14. In this case, coalescence occurs later and the void growth rate is lower.

Figure 14 also presents the prediction of the Rice-Tracey model [37] along with a simulation with a single void under the same conditions. The single void simulation is reasonably close to the Rice-Tracey prediction. The slight underestimation produced by the Rice-Tracey model is consistent with the analysis provided by Huang [38] on dilatation rates of spherical voids. The presence of a second void (simulation with no internal void) accelerates void growth and thus the result deviates from the Rice-Tracey prediction. When a third void is introduced (the rest of the simulations presented in Figure 15), the results deviate even further from the Rice-Tracey model even for large values of d_2. Given that all the simulations were carried out under the same stress triaxiality ratio, these results illustrate the importance of considering the interactions between voids in heterogeneous arrangements.

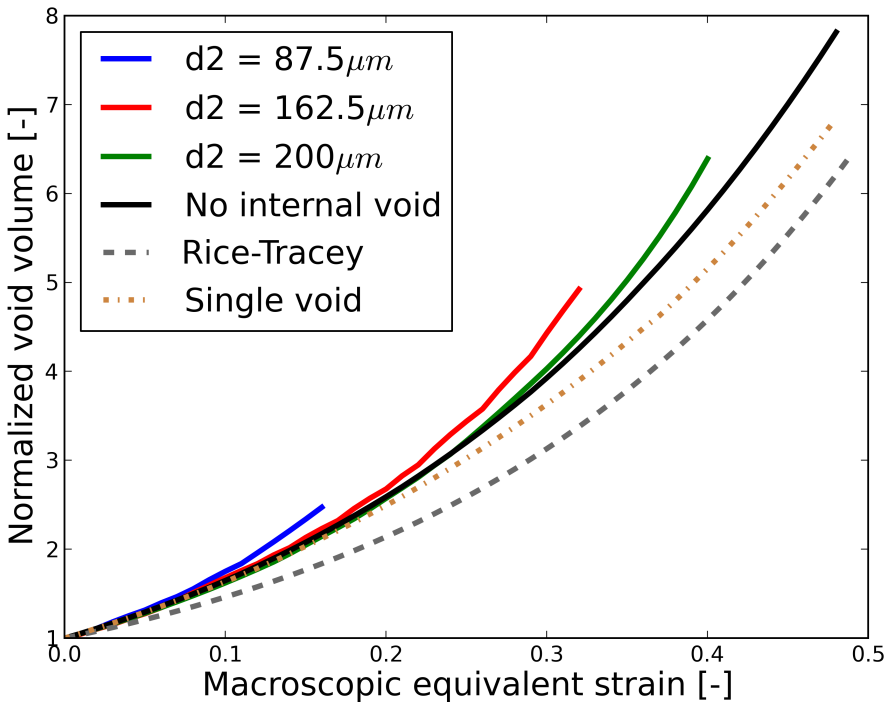

Figure 14: Effect of the internal void on the growth of the external void.

Figure 15 depicts the final configuration after coalescence of the void cluster in the presence of the internal void (Figure 15a) and in the absence of the internal void (15b). When the internal void is present, coalescence between the internal void and the external voids occurs very early (imposed equivalent strain of 0.11). In the absence of the internal void, coalescence between the external voids occurs much later (imposed equivalent strain of 0.46), i.e., four times later than in the presence of the internal void. The appearance of the coalesced voids in Figure 15b resembles the experimental observations of Weck and Wilkinson [39] in metallic sheets with laser drilled holes when the holes were oriented at 45 deg with respect to the loading direction; the voids first undergo considerable volume change by mainly elongating in the loading direction, and then present coalescence far from their equator.

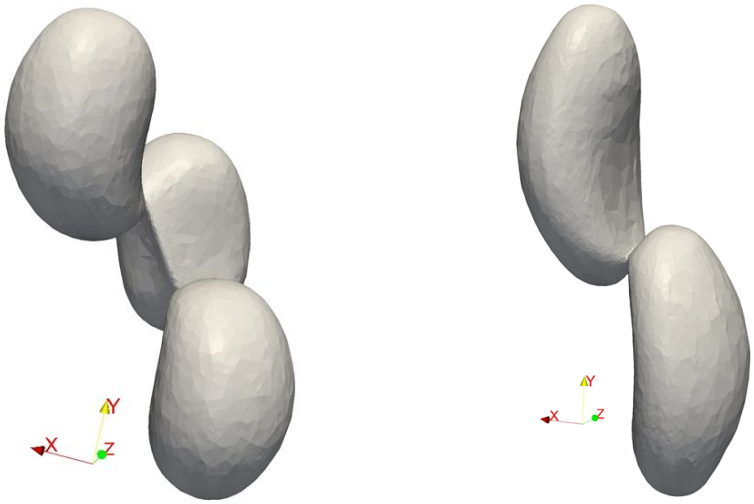

(a) With internal void ($d_2 = 1$)

(b) Without internal void

Figure 15: Final configuration of voids after coalescence.

3.3 Effect of d_1

This section describes how the evolution of normalized void volume, minimum intervoid distance and plastic strain in the middle point between the

shortest path between voids, changes with d_1 for a fixed value of d_2 of 1.75; the position of the internal void will be fixed and the external voids will change their position (sense indicated in green in Table 1). Four cases are examined. The fourth case ($d_1 = 3.25$), does not present coalescence up to the end of the simulation which corresponds to a final macroscopic equivalent strain of 0.5.

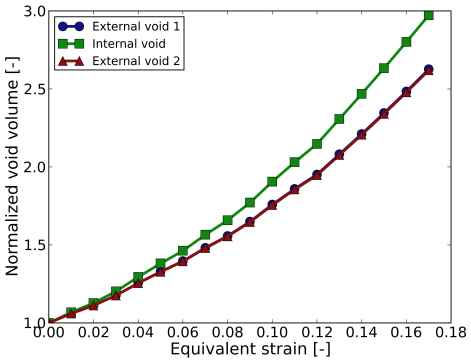

(a) $d_1 = 1$

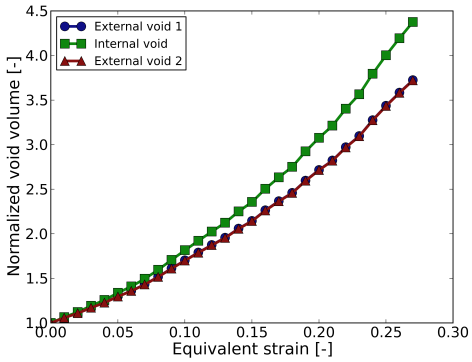

(b) $d_1 = 1.75$

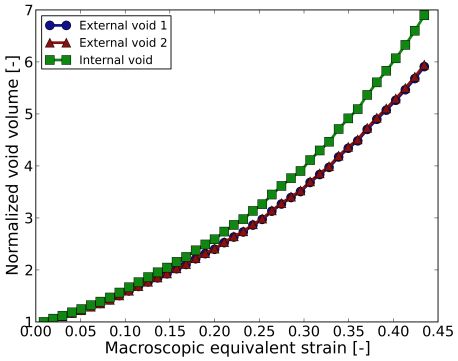

(c) $d_1 = 2.5$

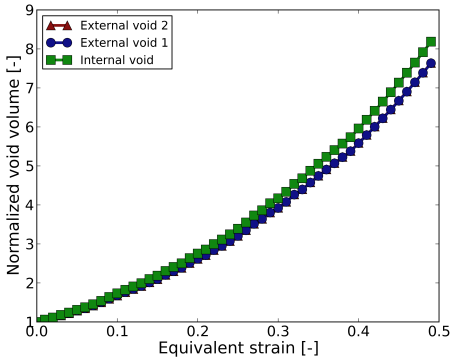

(d) $d_1 = 3.25$

Figure 16: Effect of d_1 on the normalized void volume for a fixed value of $d2 = 1.75$.

The way how the evolution of void volume changes with d_1, is depicted in Figure 16. In all cases an exponential increase is observed, and the increase of the internal void volume is superior to that of the external voids. The

difference of normalized void growth between the internal and external voids increases with d_1 and goes from 0.3 when $d_1 = 1$ (Figure 16a) to 0.95 when $d_1 = 2.5$ (Figure 16c).

Figure 17 demonstrates the effect of d_1 on the evolution of the minimum intervoid distance. In these four cases, the initial intervoid distance in the external-external pair is greater than that of the internal-external pair. The internal-external pair presents a higher rate of decrease. The curves change in a similar manner when d_1 is increased: an accelerated decrease of the intervoid distance is observed for lower values of d_1, and it decreases more linearly as d_2 increases.

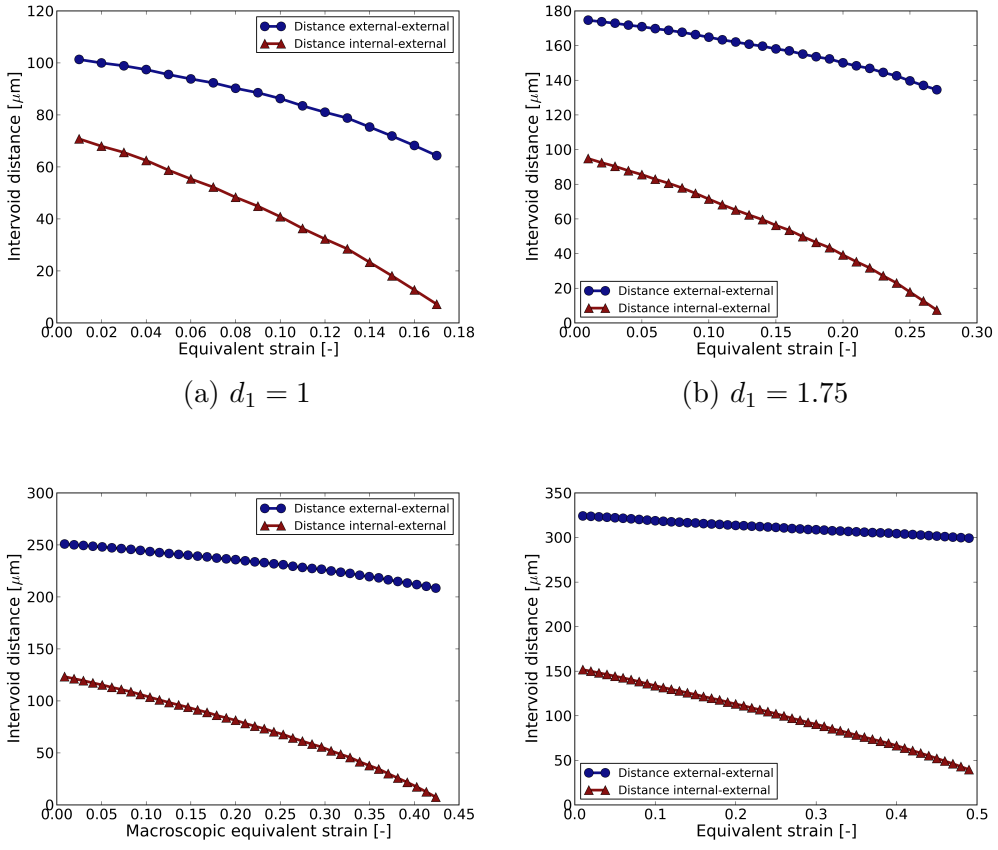

(a) $d_1 = 1$ (b) $d_1 = 1.75$

(c) $d_1 = 2.5$ (d) $d_1 = 3.25$

Figure 17: Effect of d_1 on the minimum intervoid distance for a fixed value of $d2 = 1.75$.

The effect of d_1 on the evolution of the equivalent plastic strain at the middle point of the shortest paths between voids, is illustrated in Figure 18. For both pairs, the evolution of the equivalent strain is exponential for low values of d_1 and transitions towards linearity when d_1 increases. The value of the macroscopic equivalent strain at coalescence increases monotonically with increasing d_1. The cases with $d_1 = 1$ and $d_1 = 1.75$ present, like the cases in section 3.2, a value of equivalent strain at coalescence in the middle of the internal-external in the range between 2.5 and 3.0. The case with $d_1 = 2.5$ presents a higher value with 3.8, and case with $d_1 = 3.25$ presents no coalescence and a smaller value of plastic strain of 1.7.

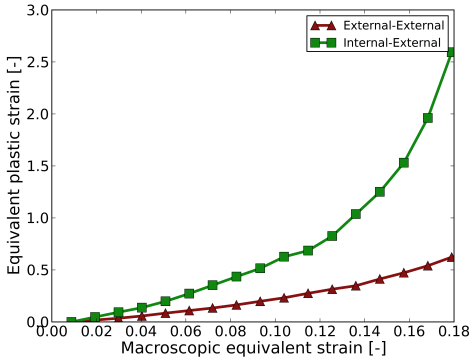

(a) $d_1 = 1$

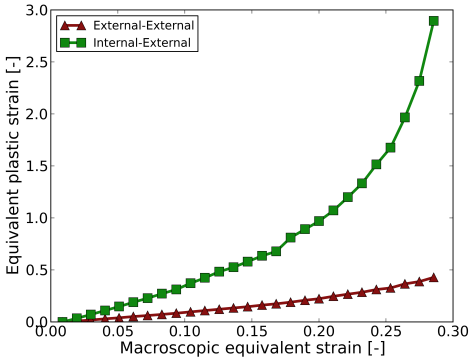

(b) $d_1 = 1.75$

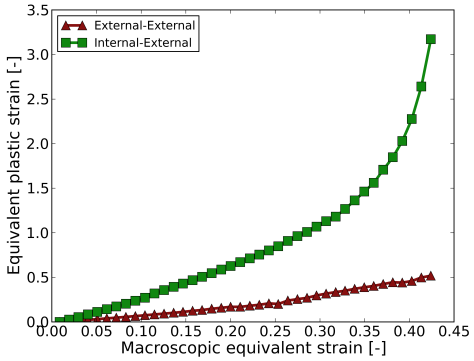

(c) $d_1 = 2.5$

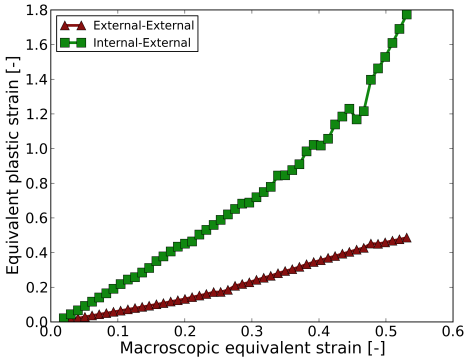

(d) $d_1 = 3.25$

Figure 18: Effect of d_1 on the equivalent plastic strain at middle point of shortest path between voids for a fixed value of $d2 = 1.75$.

3.4 Global results and discussion

In Figure 19, a response surface is depicted. This response surface presents the macroscopic equivalent strain at coalescence as a function of d_1 and d_2. Accomplished simulations are indicated as a blue dot. The white zones indicate that coalescence was not observed up to the end of the simulation, i.e., up to 0.5 of macroscopic equivalent strain. Coalescence was observed for a wide range of strains: from 0.1 up to 0.5.

The parametric space could be explored more assiduously if the presented coalescence mechanisms is to be described more in detail. In particular, the transitions between the parameter combinations that exhibit coalescence and those that don't should be further explored if quantitative information is to be used. However, the objective of the parametric study was to show that the coalescence mechanisms between three voids can be observed for many different initial configurations. Figure 19 demonstrates that this mechanism is obtained for a wide range of values of d_1 and d_2 given that the domain is sufficiently deformed.

The acceleration increase of the local equivalent strain with respect to the far-field strain has already been reported in the work of Bandstra and Koss [27] for a Gurson material model; the authors observed a more complex localization behavior. The use of an elastic-perfectly plastic material in this work highlighted the interaction of the voids while neglecting the effect of secondary voids, which was desirable to study the hypothesis that three dimensional interactions could lead to apparent void-sheet coalescence instances. The introduction of strain hardening and/or softening due to a secondary population of voids would change the observed trends and constitutes a perspective of this work.

The detailed description of the coalescence in the cluster suggests the utilization of two of the employed observables as coalescence criterion: the equivalent strain at coalescence at the middle point of the shortest path be-

tween voids, and the minimum distance between voids. The former was used by Bandstra and Koss [27] to construct a failure limit diagram; the value the authors used as threshold was based on the nucleation strain for secondary particles. As seen in sections 3.2 and 3.3, most of the observed coalescence instances in the parametric study present a local strain before coalescence in the range of 0.25-0.3. The latter provides a very natural threshold for coalescence by internal necking: coalescence occurs when the minimum intervoid distance for a pair of voids reaches zero. The simple trends observed for this variable in the results of the simulations, are promising in the sense that they could be described with simple evolution laws. An extended parametric study considering various numbers of voids, mechanical behaviors and stress states, could help identify a proper threshold for the local strain or help formulate evolution laws for the minimum intervoid distance. These two possibilities will be explored in future work.

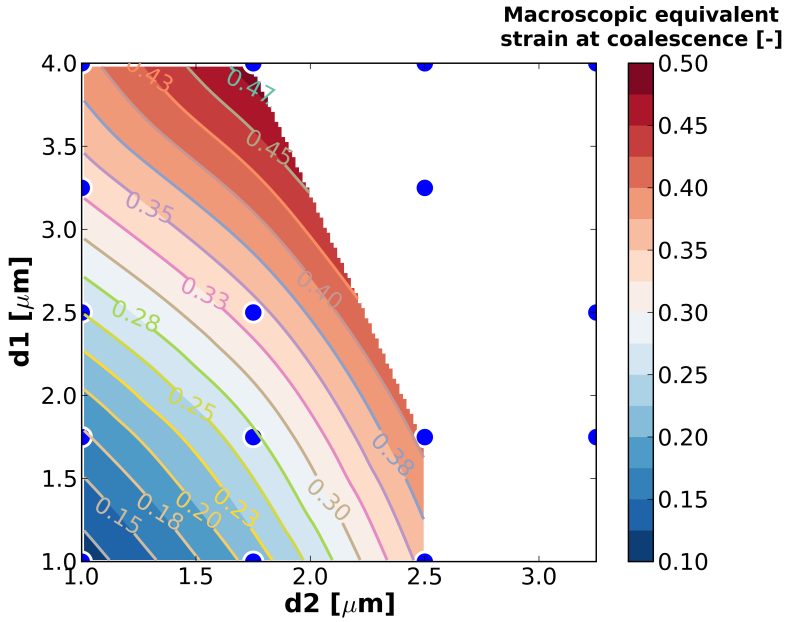

Figure 19: Equivalent strain of the domain at coalescence as a function of d_1 and d_2. The blue dots indicate the accomplished simulations.

4 Conclusions and perspectives

A methodology for the study of three-dimensional non-periodic clusters of voids and/or particles was proposed as a complementary approach in the study of the micromechanisms of ductile damage.

The proposed methodology was put in use to assess if the interaction with neighboring voids could play a role in apparent void-sheet instances observed in different materials. The FE simulations of a cluster with three voids show that accelerated and non-homogeneous void growth is promoted in the vicinity of the plastic localization band; a high curvature region that grows towards the localization band is formed. The coalescence mechanism between the voids corresponds to internal necking.

If a two-dimensional cut of the voids after coalescence is made, the resulting image considerably resembles the experimental observations. This supports the hypothesis that three dimensional interactions can play a role in the apparent void sheet instances. More generally, these results point at the importance of considering three-dimensional and non-periodic phenomena in the study of ductile damage at the microscale.

The predictions of the Rice-Tracey void growth model were compared with simulations with one, two, and three voids. When one void is considered, the results of the simulation are close to the Rice-Tracey prediction. When two or three voids are simulated, the Rice-Tracey model deviates significantly from the results of the numerical results. This highlights the importance of considering the effect of intervoid interactions in non-simplified configurations.

Although the use of an elastic-perfectly plastic material was useful for the study of the proposed hypothesis -that three dimensional interactions between voids can give origin to coalescence mechanisms that resemble the void-sheet mechanism-, a perspective of this work is to study the effect of

strain hardening and softening due to damage at smaller scales, on the described coalescence mechanism. Other stress states will also be studied.

The results of the parametric study provided a detailed description of the void growth and coalescence of the studied three voids cluster and the effect of the initial configuration on the coalescence was studied. It was observed that under an identical far-field stress, the growth undergone by a void depends on its relative position in the cluster. Further work is necessary to better understand the complex interactions between voids in realistic clusters.

Results from the parametric study suggest that the equivalent plastic strain at the middle point of the shortest path between voids or the evolution of the minimum intervoid distance, might be appropriate coalescence indicators. Future work will investigate these possibilities via the herein proposed methodology for different configurations, mechanical behaviors and stress states.

Acknowledgements

This work was performed within the COMINSIDE project funded by the French Agence Nationale de la Recherche (ANR-14-CE07-0034-02 grant).

References

[1] A. Pineau, A. A. Benzerga, and T. Pardoen, "Failure of metals i: Brittle and ductile fracture," *Acta Materialia*, vol. 107, pp. 424–483, 2016.

[2] A. A. Benzerga and J.-B. Leblond, "Ductile fracture by void growth to coalescence," *Advances in Applied Mechanics*, vol. 44, pp. 169–305, 2010.

[3] T. Cox and J. R. Low, "An investigation of the plastic fracture of aisi 4340 and 18 nickel-200 grade maraging steels," *Metallurgical and Materials Transactions B*, vol. 5, no. 6, pp. 1457–1470, 1974.

[4] D. Goto, D. Koss, and V. Jablokov, "The influence of tensile stress states on the failure of HY-100 steel," *Metallurgical and Materials Transactions A*, vol. 30, no. 11, pp. 2835–2842, 1999.

[5] J. Gammage, D. Wilkinson, J. Embury, and E. Maire, "Damage studies in heterogeneous aluminium alloys using x-ray tomography," *Philosophical Magazine*, vol. 85, no. 26-27, pp. 3191–3206, 2005.

[6] A. Weck, D. Wilkinson, and E. Maire, "Observation of void nucleation, growth and coalescence in a model metal matrix composite using x-ray tomography," *Materials Science and Engineering: A*, vol. 488, no. 1, pp. 435–445, 2008.

[7] E. Maire, S. Zhou, J. Adrien, and M. Dimichiel, "Damage quantification in aluminium alloys using in situ tensile tests in X-ray tomography," *Engineering Fracture Mechanics*, vol. 78, no. 15, pp. 2679–2690, 2011.

[8] Y. Shen, T. F. Morgeneyer, J. Garnier, L. Allais, L. Helfen, and J. Crépin, "Three-dimensional quantitative in situ study of crack initiation and propagation in AA6061 aluminum alloy sheets via synchrotron laminography and finite-element simulations," *Acta Materialia*, vol. 61, no. 7, pp. 2571–2582, 2013.

[9] L. Babout, E. Maire, and R. Fougeres, "Damage initiation in model metallic materials: X-ray tomography and modelling," *Acta Materialia*, vol. 52, no. 8, pp. 2475–2487, 2004.

[10] A. Buljac, M. Shakoor, J. Neggers, M. Bernacki, P.-O. Bouchard, L. Helfen, T. F. Morgeneyer, and F. Hild, "Numerical validation framework for micromechanical simulations based on synchrotron 3D imaging," *Computational Mechanics*, vol. 59, no. 3, pp. 419–441, 2017.

[11] M. Shakoor, A. Buljac, J. Neggers, F. Hild, T. F. Morgeneyer, L. Helfen, M. Bernacki, and P.-O. Bouchard, "On the choice of boundary conditions for micromechanical simulations based on 3D imaging," *International Journal of Solids and Structures*, vol. 112, pp. 83–96, 2017.

[12] A. Buljac, L. Helfen, F. Hild, and T. F. Morgeneyer, "Effect of void arrangement on ductile damage mechanisms in nodular cast iron: in situ 3D measurements," *Manuscript submitted for publication.*

[13] M. Shakoor, M. Bernacki, and P.-O. Bouchard, "A new body-fitted immersed volume method for the modeling of ductile fracture at the microscale: Analysis of void clusters and stress state effects on coalescence," *Engineering Fracture Mechanics*, vol. 147, pp. 398–417, 2015.

[14] M. Shakoor, P.-O. Bouchard, and M. Bernacki, "An adaptive level-set method with enhanced volume conservation for simulations in multiphase domains," *International Journal for Numerical Methods in Engineering*, vol. 109, no. 4, pp. 555–576, 2017.

[15] M. Shakoor, B. Scholtes, P.-O. Bouchard, and M. Bernacki, "An efficient and parallel level set reinitialization method–application to micromechanics and microstructural evolutions," *Applied Mathematical Modelling*, vol. 39, no. 23, pp. 7291–7302, 2015.

[16] E. Roux, M. Bernacki, and P.-O. Bouchard, "A level-set and anisotropic adaptive remeshing strategy for the modeling of void growth under large plastic strain," *Computational Materials Science*, vol. 68, pp. 32–46, 2013.

[17] F. Brezzi, D. Boffi, L. Demkowicz, R. Durán, R. Falk, and M. Fortin, *Mixed finite elements, compatibility conditions, and applications*. Springer, 2008.

[18] A. Needleman, "Void growth in an elastic-plastic medium," in *Journal of Applied mechanics*, ASME, 1972.

[19] V. Tvergaard, "Influence of voids on shear band instabilities under plane strain conditions," *International Journal of Fracture*, vol. 17, no. 4, pp. 389–407, 1981.

[20] C. Thomson, M. Worswick, A. Pilkey, D. Lloyd, and G. Burger, "Modeling void nucleation and growth within periodic clusters of particles," *Journal of the Mechanics and Physics of Solids*, vol. 47, no. 1, pp. 1–26, 1998.

[21] C. Thomson, M. Worswick, A. Pilkey, and D. Lloyd, "Void coalescence within periodic clusters of particles," *Journal of the Mechanics and Physics of Solids*, vol. 51, no. 1, pp. 127–146, 2003.

[22] C. McVeigh, F. Vernerey, W. K. Liu, B. Moran, and G. Olson, "An interactive micro-void shear localization mechanism in high strength steels," *Journal of the Mechanics and Physics of Solids*, vol. 55, no. 2, pp. 225–244, 2007.

[23] V. Tvergaard, "Effect of void cluster on ductile failure evolution," *Meccanica*, vol. 12, no. 51, pp. 3097–3105, 2016.

[24] I. Khan and V. Bhasin, "On the role of secondary voids and their distribution in the mechanism of void growth and coalescence in porous plastic solids," *International Journal of Solids and Structures*, vol. 108, pp. 203–215, 2017.

[25] N. Ohno and J. Hutchinson, "Plastic flow localization due to non-uniform void distribution," *Journal of the Mechanics and Physics of Solids*, vol. 32, no. 1, pp. 63–85, 1984.

[26] M. Horstemeyer, M. Matalanis, A. Sieber, and M. Botos, "Micromechanical finite element calculations of temperature and void configuration effects on void growth and coalescence," *international Journal of Plasticity*, vol. 16, no. 7, pp. 979–1015, 2000.

[27] J. Bandstra and D. Koss, "Modeling the ductile fracture process of void coalescence by void-sheet formation," *Materials Science and Engineering: A*, vol. 319, pp. 490–495, 2001.

[28] J. Bandstra, D. Koss, A. Geltmacher, P. Matic, and R. Everett, "Modeling void coalescence during ductile fracture of a steel," *Materials Science and Engineering: A*, vol. 366, no. 2, pp. 269–281, 2004.

[29] V. Tvergaard and A. Needleman, "Three dimensional microstructural effects on plane strain ductile crack growth," *International journal of solids and structures*, vol. 43, no. 20, pp. 6165–6179, 2006.

[30] J. Bandstra and D. Koss, "On the influence of void clusters on void growth and coalescence during ductile fracture," *Acta Materialia*, vol. 56, no. 16, pp. 4429–4439, 2008.

[31] X. Sun, K. S. Choi, W. N. Liu, and M. A. Khaleel, "Predicting failure modes and ductility of dual phase steels using plastic strain localization," *International Journal of Plasticity*, vol. 25, no. 10, pp. 1888–1909, 2009.

[32] N. Vanderesse, E. Maire, A. Chabod, and J.-Y. Buffière, "Microtomographic study and finite element analysis of the porosity harmfulness in a cast aluminium alloy," *International Journal of Fatigue*, vol. 33, no. 12, pp. 1514–1525, 2011.

[33] S. Youssef, E. Maire, and R. Gaertner, "Finite element modelling of the actual structure of cellular materials determined by x-ray tomography," *Acta Materialia*, vol. 53, no. 3, pp. 719–730, 2005.

[34] J. A. Nelder and R. Mead, "A simplex method for function minimization," *The computer journal*, vol. 7, no. 4, pp. 308–313, 1965.

[35] S. G. Johnson, "The nlopt nonlinear-optimization package," 2014.

[36] H. Digonnet, L. Silva, and T. Coupez, "Cimlib: a fully parallel application for numerical simulations based on components assembly," in *AIP Conference Proceedings*, vol. 908, pp. 269–274, AIP, 2007.

[37] J. R. Rice and D. M. Tracey, "On the ductile enlargement of voids in triaxial stress fields," *Journal of the Mechanics and Physics of Solids*, vol. 17, no. 3, pp. 201–217, 1969.

[38] Y. Huang, "Accurate dilatation rates for spherical voids in triaxial stress fields," *Journal of Applied Mechanics*, vol. 58, p. 1084, 1991.

[39] A. Weck and D. Wilkinson, "Experimental investigation of void coalescence in metallic sheets containing laser drilled holes," *Acta Materialia*, vol. 56, no. 8, pp. 1774–1784, 2008.